Tunnelling and Underground Space Technology 83 (2019) 509–519

Contents lists available at ScienceDirect

Tunnelling and Underground Space Technology

journal homepage: www.elsevier.com/locate/tust

Collapsible characteristics of loess tunnel site and their effects on tunnel structure

Jun Li[a], Shengjun Shao[a,b,*], Shuai Shao[a]

[a] Civil Engineering and Architecture Institute, Xi'an University of Technology, Xi'an 710048, China
[b] Shaanxi Key Laboratory of Loess Mechanics and Engineering, Xi'an 710048, China

ARTICLE INFO

Keywords:
Loess tunnel
Field immersion test
Collapsible deformation
Mechanical response
Engineering measures

ABSTRACT

During the infrastructure construction process in the loess region of Northwest China, some tunnels are inevitably located in collapsible loess strata, and the potential collapsible deformation of the surrounding loess may threaten the safety and stability of the tunnel structure. To investigate the functional mechanism of loess strata hydrocollapse for a tunnel structure, a large field water immersion test was conducted in this study on the ground surface above an existing loess tunnel. The subsidence of the strata and the mechanical response of the tunnel structure during long-term water immersion were measured and analysed to reveal the collapsible deformation characteristics of the loess tunnel site and their effects on the tunnel structure. The results show that the surface water could infiltrate into the base of the tunnel and that a large deformation occurred in the surrounding loess near the tunnel vault once the loess was wetted. As the water infiltrated to the burial depth of the tunnel, the base pressure increased significantly, the tunnel structure subsided and the inverted arch cracked. Therefore, for a loess tunnel with a relatively shallow burial depth, long-term water immersion above the tunnel should be avoided, and the possibilities of decreasing bearing capacity and tunnel foundation subsidence at the arch feet caused by wetting must be considered during design and construction.

1. Introduction

Loess covers approximately 631 000 km^2 of China, which is equivalent to 6.6% of the total area of the country (Liu and Chang, 1964; Derbyshire et al., 1995). Most of these soils are formed with a loose, honeycomb-type meta-stable structure, which is susceptible to a dramatic decrease in stiffness and a large reduction in total volume upon wetting (Houston et al., 1988; Derbyshire et al., 1994; Xie, 2001). This property of loess is known commonly as hydrocollapse. In the past, engineering facilities in loess areas were frequently damaged by loess collapses, such as foundational differential settlement, earth cracks, underground pipelines ruptures, and even slides, slumps or flow masses, which directly threatened human lives (Derbyshire, 2001; Sun et al., 2013). For this reason, many researchers and engineers have carried out a large amount of research on the collapse mechanisms and quantitative methods of loess hydrocollapse (Assallay et al., 1997; Haeri et al., 2016; Li et al., 2016). The ultimate purpose of these studies is to reasonably predict the collapsible deformation of loess strata and to correctly evaluate the impacts of loess hydrocollapse for projects under different engineering conditions. This information can be used to control or avoid the damages of loess collapsibility in engineering.

Over the past six decades, according to a series of correlative research achievements and engineering practice experiences, four editions of the *Code on Building Construction in Regions of Collapsible Loess* have been published as the guideline for building construction in the loess area of China, and the present version was enacted in 2004 (MCPRC, 2004). Under the guidelines of the code, the number of building security accidents in loess areas caused by hydrocollapse has obviously decreased due to the successful evaluation of the collapse potential of loess foundations and the implementation of suitable foundation treatment measures. However, the conditions in which the methods of evaluating the loess collapsibility can be used according to code are limited because the code is mainly suitable for shallow foundations under conditions of self-weight or additional loading (Yao et al., 2014; Shao et al., 2015).

With the development of the northwestern regions and the progress resulting from the Belt and Road initiative in China, a large number of infrastructure projects, including high-speed railways, expressways and urban metros, have been completed in the loess area of Northwest China. Some tunnels inevitably pass through collapsible loess strata, and the potential collapsibility of the surrounding loess may adversely impact the safety and stability of the tunnel structure. Thus, it is

* Corresponding author at: Civil Engineering and Architecture Institute, Xi'an University of Technology, Xi'an 710048, China.
E-mail address: sjshao@xaut.edu.cn (S. Shao).

https://doi.org/10.1016/j.tust.2018.08.035
Received 12 January 2018; Received in revised form 28 June 2018; Accepted 16 August 2018

important to reasonably evaluate the collapsible deformation of the surrounding loess and determine its impact on the tunnel structure. Tunnels usually have a certain burial depth, and the stress field of the surrounding rock has been significantly changed during tunnel excavation. The collapsible deformation of surrounding loess is markedly different from the shallow foundation of a building, which is beyond the applicable scope of the code mentioned above (Shao et al., 2013). Therefore, some research regarding a reasonable evaluation method for the collapsibility of a loess tunnel has been conducted by researchers with the aim of confirming the conditions that lead to the occurrence of surrounding loess collapse and its effects on the tunnel structure. Considering the stress characteristics of a tunnel base, Li et al. (2015) proposed a calculation method for loess strata collapsible deformation under a tunnel base, and Shao et al. (2017) suggested grading standards for tunnel foundation subsidence according to the degree of impact on the tunnel structure caused by collapsible deformation. Lin et al. (2016) preliminarily revealed the interaction mechanism between a tunnel structure and the collapsible deformation of surrounding loess with the centrifugal model test, which simulated the loess collapse around a metro tunnel upon wetting. Huang (2017) and Tian (2017) studied the mechanical response of the tunnel structure under different positions and degrees of surrounding loess collapse using scale model tests and numerical simulations. These research achievements are valuable references for establishing a method for evaluating the collapsibility of loess tunnels. However, the theoretical analyses, physical model tests and numerical simulations do not fully represent the actual conditions of a practical project.

In this study, a large water immersion test was conducted in the field with a testing pit that covered an area of 800 m^2 on the ground surface directly above an existing loess tunnel (Fig. 1), which is rare in China and around the world. The settlement of loess strata and the mechanical response of the tunnel structure during long-term water immersion were measured and analysed. The results reveal the collapsible deformation characteristics of the loess tunnel site and the effects of the loess hydrocollapse on the tunnel structure under the actual stress conditions of the surrounding rock after tunnel construction.

2. Geological conditions and test overview

2.1. Geological conditions

An inclined shaft (temporary construction tunnel) located in the Yuzhong Country of Lanzhou, China, was selected as the test site. The inclined shaft is a horseshoe-shaped tunnel with a height of 7.6 m and a span of 7.2 m. The total length of the tunnel is approximately 200 m, the average slope is approximately 13.5%, and the burial depth ranges from 11 m to 56 m. As an auxiliary gallery, the tunnel has only a single lining structure with a thickness of 40 cm composed of steel arch frames and anchor sprayed concrete, which was built 2 years before this test.

This test site is located in loess mountainous terrain. Field exploration revealed that the strata to a depth of 80 m is mainly composed of Late Pleistocene Malan loess (Q_3^{al}) and Middle Pleistocene Lishi loess (Q_2^{eol}), and the thickness of the collapsible loess layer is approximately 30 m. No groundwater was found within the depth of exploration. Table 1 shows the basic parameters of the loess strata within a depth of 40 m at the test site. Based on the field conditions, including the thickness of the collapsible soil layer, the size of the actual test site and the relative burial depth of the tunnel, a rectangular water immersion

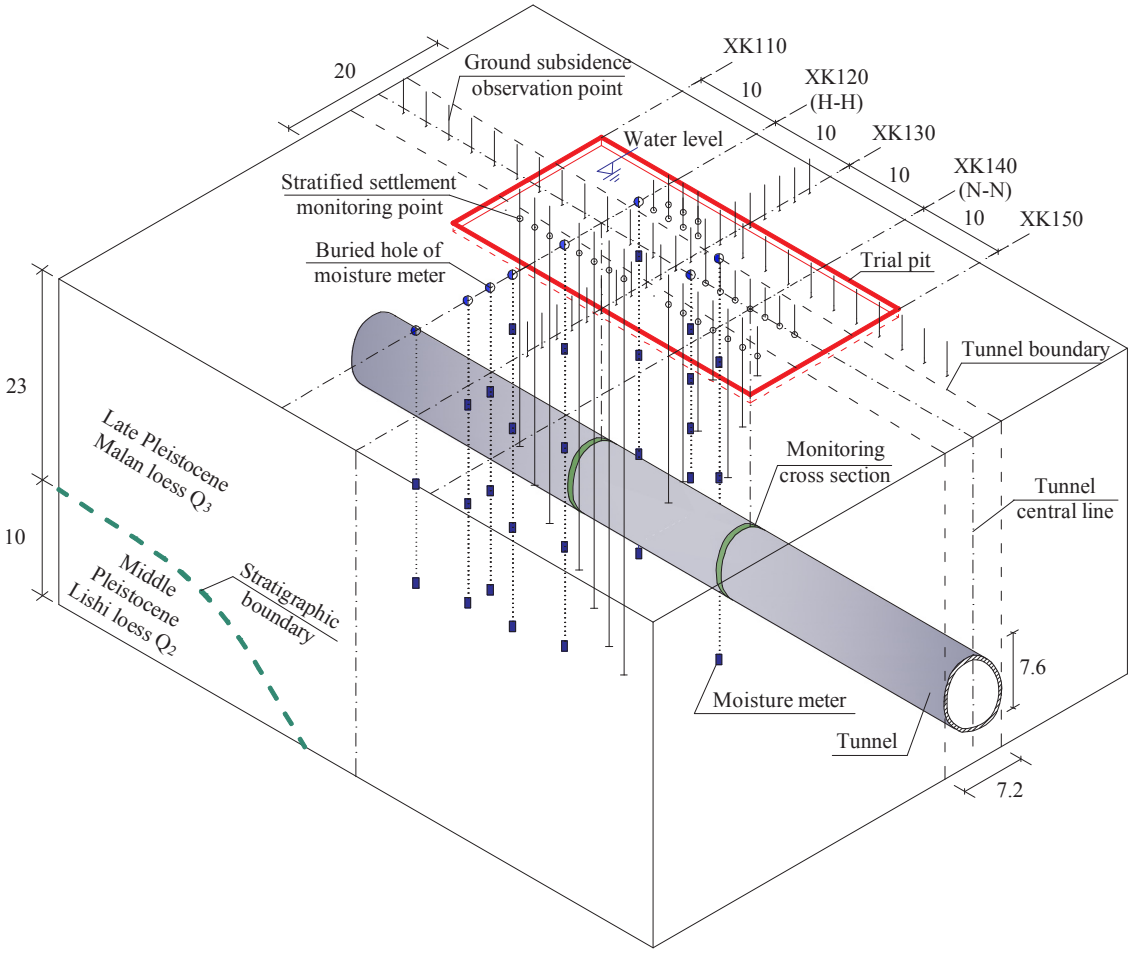

Fig. 1. Diagram of the field water immersion test above a loess tunnel (unit: m).

Table 1
Distribution and physical parameters of soil layers.

Strata	Thickness, h/m	Moisture content, w/%	Dry density, ρ_d/(g/cm^3)	Void ratio, e	Maximum self-weight collapsibility coefficient, δ_{zs}
Malan loess (Q_3^{al})	0–35	5.0–20.4	1.25–1.45	1.16–0.86	0.087
Lishi loess (Q_2^{eol})	28–40	18.8–21.3	1.36–1.47	0.99–0.84	0.030

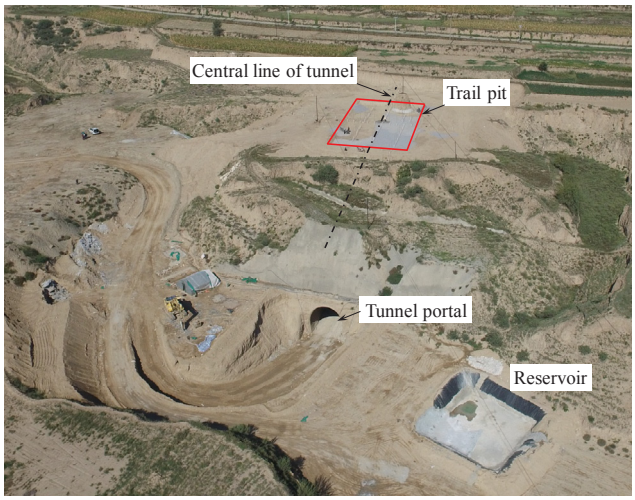

Fig. 2. General view of test site (imaged by authors).

trial pit (40 m long, 20 m wide and 0.6 m deep) was placed on the ground surface above the tunnel, and the centre line of the pit coincided with the longitudinal axis of the tunnel. The test pit location corresponded to the tunnel mileage of XK110–XK150 (Fig. 1). A general view of the test site is shown in Fig. 2.

2.2. Test monitoring scheme

2.2.1. Monitoring points around the trial pit

To measure the strata settlement and the distribution pattern of water infiltration during the immersion test, a series of subsidence monitoring points and TDR soil moisture meters were installed in different locations (Fig. 3).

The subsidence monitoring points were divided into two categories, including 42 ground subsidence monitoring points and 28 stratified settlement monitoring points. The former monitoring points were installed along four directions from the centre of the pit, which were labelled A1–A9, B1–B12, C1–C10, and D1–D10, and the label of the central point was O. The latter monitoring points were labelled F1–F28 and were installed at depths ranging from 2 m to 40 m with a vertical spacing of 3 m. F1–F7 (2–20 m) were located above the tunnel and the F8–F28 (2–40 m) monitoring points were located on both sides of the tunnel.

A TDR soil moisture meter can reflect the variations in soil volumetric water content (θ_v) by measuring the changes in the apparent dielectric constant (ε) of the soil (Huang et al., 2012; Cristi et al., 2016). There were 34 soil moisture meters distributed in 12 drill holes (labelled W1–W12), including 16 soil moisture meters in the pit (W1–W4) and 18 soil moisture meters outside the pit (W5–W12). The embedded depths ranged from 5 m to 40 m, with an interval of 5 m, and each depth in the pit included 2 soil moisture meters, which is shown in Fig. 3 and Fig. 4.

2.2.2. Monitoring points in tunnel structure

To obtain the mechanical response of a tunnel structure caused by long-term water infiltration from the ground surface, two cross sections of the tunnel under the trial pit, which correspond to mileage XK 120 and XK 140, were chosen to install vibrating string earth pressure cells, vibrating string rebar stress gauges (with diameters of 22 cm) and subsidence monitoring points. The relative depth between the monitoring sections and the surface trial pit is shown in Fig. 5, and the positions of these measurement points in each section are shown in Fig. 6.

The primary lining of the tunnel was completed before this test, and thus, the earth pressure cells were installed at the interface between the primary and second linings. The rebar stress gauges were welded in the rebar cage of the second lining during the tunnel's construction (Fig. 7). These sensors were symmetrically distributed at seven positions, including the vault, spandrels, haunches and arch feet of the tunnel, which were used to measure the variations in the contact pressure between the lining structures and the internal force of the second lining structure during the immersion test. After the completion of the second lining, subsidence monitoring points were installed on both sides of the spandrel and at the centre of the inverted arch in each section. The relative altitude variations at the monitoring stations were measured by the total-station to reflect the subsidence of the tunnel structure during the immersion test. In addition, four earth pressure cells were embedded in the two monitoring sections in the soil layer beneath the inverted arch to acquire the tunnel's variations in base pressure.

2.3. Process of water supply

There was no available water source near the test site, and thus, a few water trucks were used to transport water during the immersion test. After the water was transported to the site, it was stored in a prebuilt reservoir and then pumped to the surface trial pit (Fig. 8). Due to the limited transport capacity of the water trucks (the maximum quantity of water supply per day was 200 m^3), bad weather such as rain or snow, and a power outage at the test site, a continuous water supply could not be maintained; thus, intermittent immersion was performed. The soaking test began on October 6, 2016, and the water supply stopped on January 3, 2017 (lasted 90 days). The total quantity of water supplied was 8673 m^3. The monitoring work continued until March 5, 2017. An average strata subsidence rate over five consecutive days of less than 1 mm/day and a lack of obvious change in the sensors were the criteria used to determine when to end the test.

3. Test results and analysis

3.1. Characteristics of water infiltration

The variations in the volumetric water contents of the strata at different depths that were obtained from the soil moisture meters within the trial pit are shown in Fig. 9. The volumetric water content of each soil layer began to change when the water infiltrated to the corresponding burial depth, and thus, the variation curves of the water content lagged gradually with an increase in depth. The variation curves of the water content within the depth range of 15 m show a similar pattern, which mainly include five stages: a horizontal segment before water infiltration, a drastic increase when the water arrives, a slight decrease after reaching a peak, a relatively stable stage before the water is cut off and a slow decrease after the water is cut off. Nevertheless, over the depth range of 15 m, the variation curves are roughly composed of only three stages and lack the two decreasing stages.

These changes in volumetric water content reflect that the soil was wetted at first during water infiltration. Collapsible deformation was

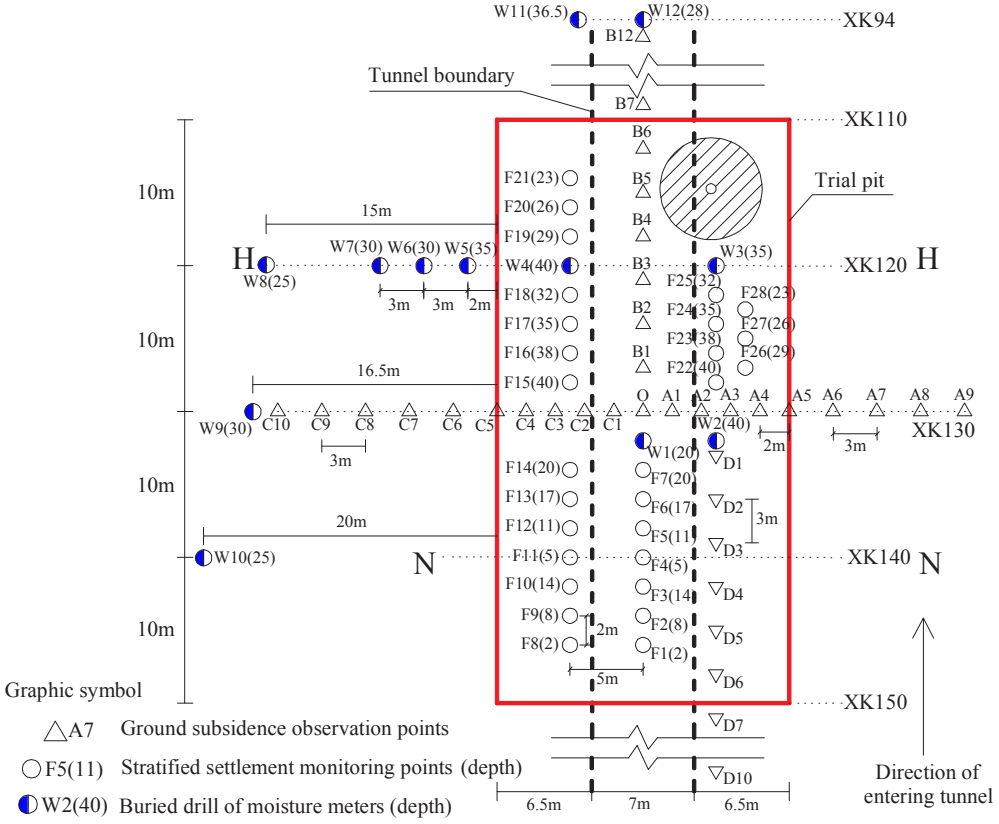

Fig. 3. Distribution of monitoring points around the trial pit (unit: m).

triggered when the moisture content of the soil increased to a certain extent, which caused soil compression and decreased the soil porosity. Thus, the volumetric water content slightly decreased with water drainage but the soil was still in the saturated state. After the water was cut off, the moisture content decreased gradually due to water migration and dissipation, and finally, the water reached a new stable state. When the depth was greater than 15 m, due to the greater density of the deeper strata, the water infiltration rate was relatively slow, and the degree of soil compaction caused by hydrocollapse was relatively small or even no collapsible deformation occurred. Therefore, when the

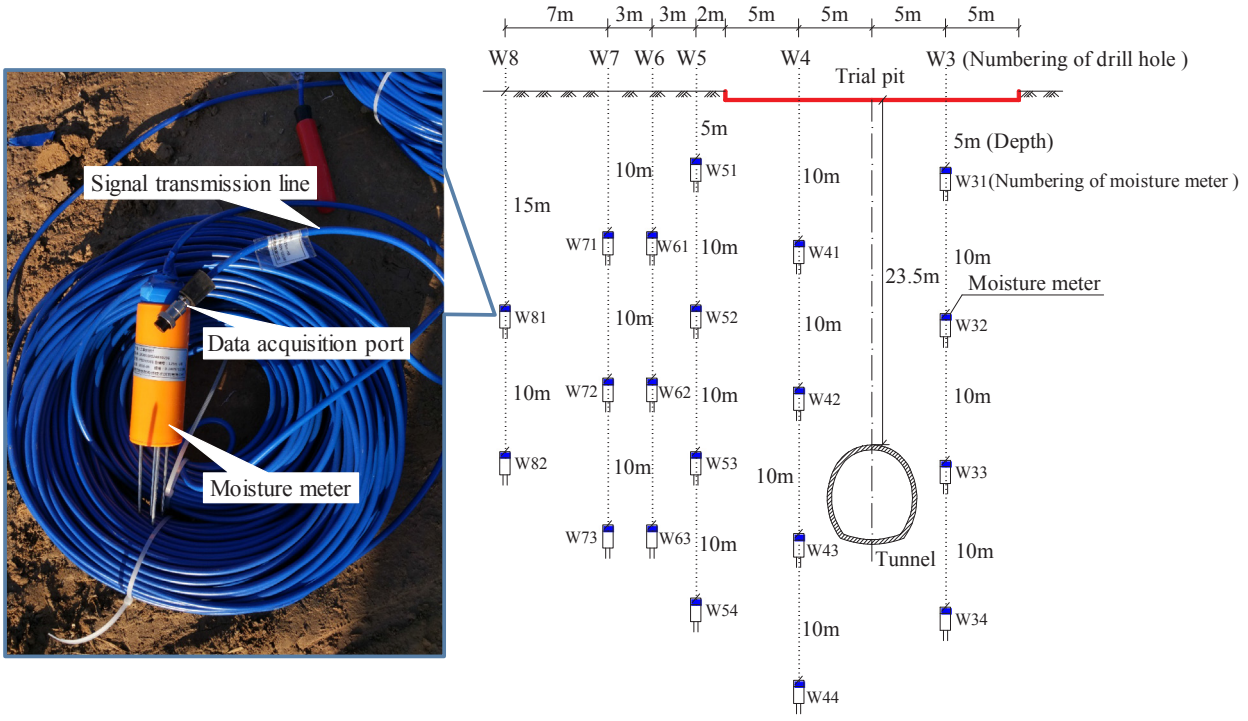

Fig. 4. Vertical view of moisture meters distribution in H-H section.

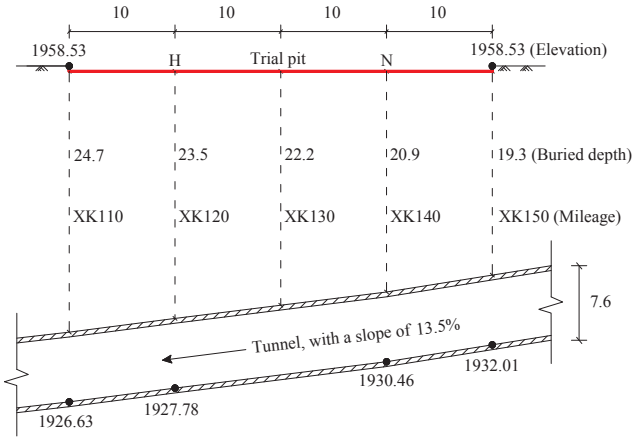

Fig. 5. The relative position between trail pit and monitoring section of tunnel (unit: m).

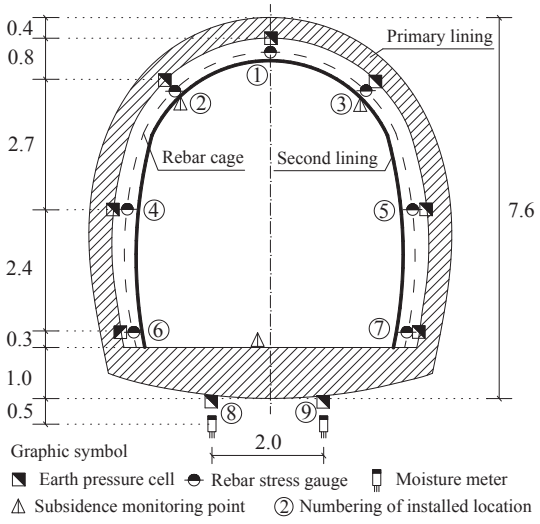

Fig. 6. Distribution and numbering of monitoring points in the tunnel (unit: m).

Fig. 8. Water injection in trial pit (imaged by authors).

water infiltrated into the deep loess layer, the volumetric water content of the soil gradually increased to its peak at a relatively slow rate and then remained stable.

Synthesizing the variation time for all moisture meters at different positions, the spatial distribution of the infiltration front during the immersion test can be speculated (Fig. 10). Fig. 10 shows that the water in the trial pit mainly infiltrates along the vertical direction, while the horizontal penetration distance is small. Before the infiltration front arrived at the burial depth of the tunnel, the permeability region pattern formed an ellipse, which was elongated along the vertical direction as the immersion time increased. After the infiltration front arrived at the burial depth of the tunnel and due to the impeded effect of the tunnel structure, the water permeated into the surrounding rock along both sides of the tunnel and continued to migrate downward. Therefore, the area influenced by immersion eventually became the shape of a 'lamp bulb'. The maximum influence depth of the water infiltration was 35 m, and the horizontal diffusion distance was approximately 5 m. In addition, an exploratory trench with a depth of 3 m was excavated near the pit boundary after the soaking test. The trench showed that the angle between the seepage line and the vertical direction was approximately 45° in the superficial stratum (Fig. 11)

Based on the time interval of the infiltration front arriving at different depths in the soil layer, the vertical infiltration rates of the water

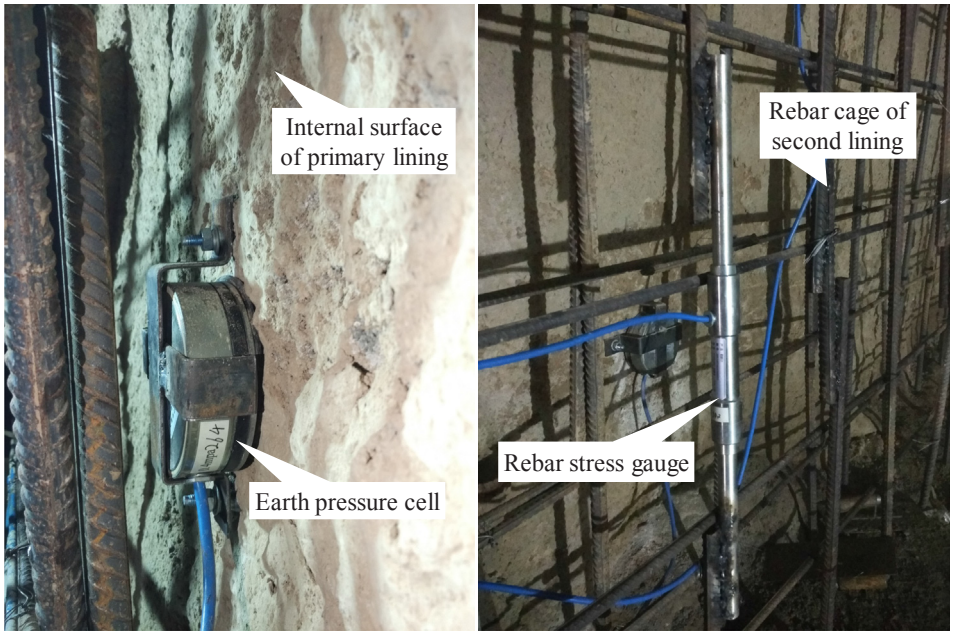

Fig. 7. Pressure cell and rebar stress gauge installed in the secondary lining (imaged by authors).

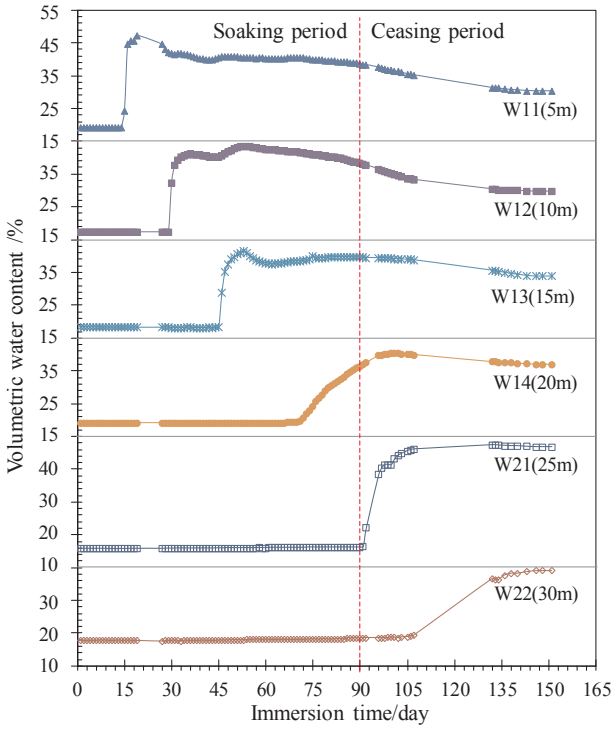

Fig. 9. Changing curves of volumetric water content of part strata at different depth within the trial pit.

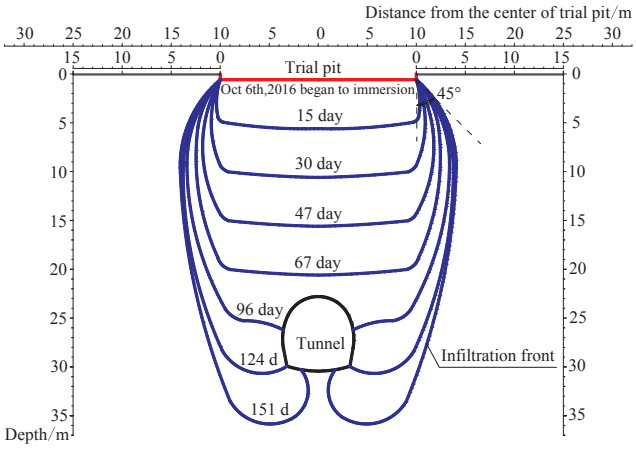

Fig. 10. Variation process of infiltration front during immersion test.

at different depths during the immersion test can be estimated as follows:

$$v_i = \frac{h_i - h_{i-1}}{t_i - t_{i-1}} \frac{\Delta h}{\Delta t} \tag{1}$$

where h_i is the water infiltration depth and t_i is the time when the seepage line arrives at the depth of h_i. In this study, $\Delta h = 5$ m, which indicates that the vertical infiltration rates of water at this site change between 3.86×10^{-4} cm/s and 2×10^{-4} cm/s, as shown in Table 2.

Previous studies suggested that the maximum impact depth of the surface water infiltration in natural loess sites (without tunnel) is generally less than 25 m (Yao et al., 2012; Huang and Yang, 2013; Wang et al., 2014), while the water infiltration depth in this study (a loess site with a tunnel passing through) was approximately 35 m, which is far deeper than that in previous studies. Meanwhile, the variation in the water infiltration rate in this study is also quite different from the variations obtained from previous immersion tests at natural loess sites (Fig. 12). For natural loess sites, the water infiltration rate dramatically decreased with increasing strata depth and became small enough when the water infiltrated to a certain depth where further permeation no longer occurred. In this study, although the infiltration rate was relatively small in the shallow strata due to the limited water supply, it did not show a significant decrease with increasing strata depth, and the surface water could easily permeate the deeper strata.

This finding reflects that the overlying loess strata was disturbed by the tunnel excavation. The vertical joint fissures of the natural loess were further developed and even formed slip bands, which changed the originally closed environment of exhaust and drainage, and the vertical permeability of the deep loess was enhanced. Thus, the infiltration rate did not obviously decrease during water infiltration. In addition, the non-tight interface between the tunnel structure and surrounding rock and the vertical crevices in the surrounding loess on both sides of the tunnel, which were caused by lateral unloading during excavation, provided convenient conditions for water migrating into the deeper soil layer. Eventually, the water on the ground surface could infiltrate into the soil layer under the tunnel base, which indicates that the excavation disturbance of the loess tunnel increases the water seepage depth on the ground surface.

3.2. Collapsible deformation of strata

3.2.1. Cracks around the trial pit

During the immersion test, multiple annular cracks gradually formed around the trial pit due to the collapsible deformation of strata, and the final pattern of crack distribution is shown in Fig. 13. From the pattern of crack distribution, the annular cracks are next to each other and gradually diverge outward. The annular cracks did not appear overnight; they followed a slow development process. During the initial soaking period, the collapsible deformation of the ground surface slowly developed, and there no cracks were generated around the trial pit. As the soaking time increased, the collapsible deformation of the strata within the trial pit developed remarkably, the ground surface near the boundary of the trial pit was fractured by tensile action, and cracks appeared in these areas. Then, the cracks gradually connected to each other as an annulus. Meanwhile, a stair-step terrain was formed along the crack due to the differential settlement between the two sides of the crack. As the scope of hydrocollapse increased, the cracks and stair-step terrains gradually extended outward layer after layer until the collapse was stable. The maximum width of the cracks is approximately 20 cm, and the maximum height of vertical dislocation is 50 cm. The farthest distance between the cracks and the boundary of the trial pit was 8.9 m (Fig. 13). Due to the non-uniform distribution of soil layers, significant differential settlement occurred on the ground surface along the longitudinal direction of the trial pit. The subsidence of the half-side of the trial pit near the tunnel portal was large, and subsidence was small on the other side. Thus, more surface cracks were distributed in the side of the trial pit near the tunnel portal, and the development of annular cracks occurred mainly around the settlement centre rather than at the boundary of the trial pit.

3.2.2. Surface subsidence

According to the monitoring data of ground subsidence observation points along the A-C axes and the infiltration front development mentioned above, the pattern variations in the surface subsidence with water infiltration of the trial pit middle cross section are depicted in Fig. 14. In Fig. 14, the infiltration fronts are shown as dashed lines, and the surface subsidence curves are shown as solid lines and correspond with different times. Fig. 14 also shows that the surface subsidence developed slowly during the initial period of soaking, and only a small amount of deformation appeared in the middle of the trial pit when water infiltrated to the depth of 5 m (pattern ①). With further immersion, obvious collapse occurred and rapidly developed under the wetting and saturated self-weight of the overlying strata. The surface

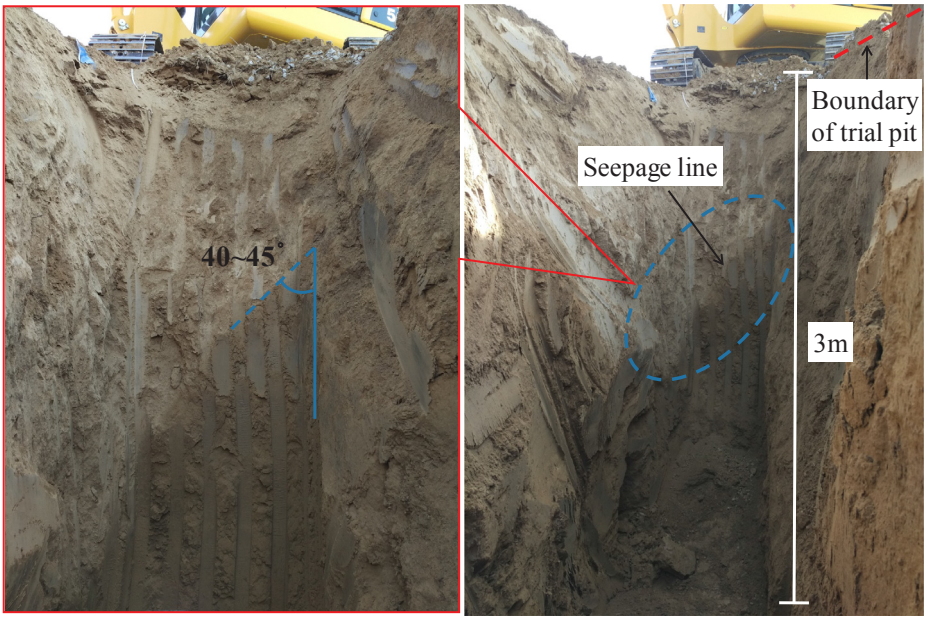

Fig. 11. The pattern of seepage line in shallow layer (imaged by authors).

Table 2
Vertical infiltration rates of water in different depths.

Infiltration depth/m	Arrival time/ (Month/Day/ Year)	Time interval/d	Infiltration rate/(10^{-4} cm/s)
5	Oct. 20th, 2016	15	3.86
10	Nov. 4th, 2016	15	3.86
15	Nov. 21th, 2016	17	3.40
20	Dec. 11th, 2016	20	2.89
25	Jan. 9th, 2017	29	2.00
30	Feb. 6th, 2017	28	2.07
35	Mar. 5th, 2017	27	2.14

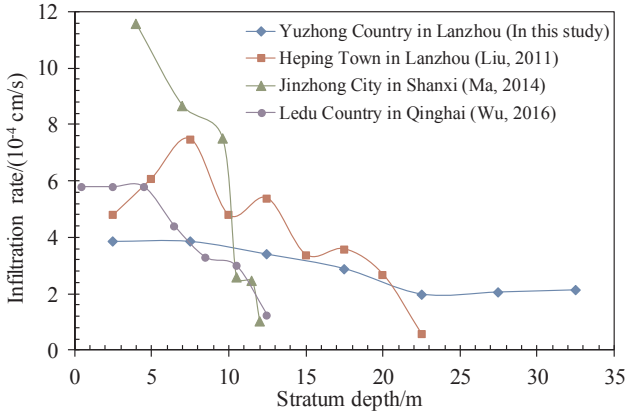

Fig. 12. Comparison of measured water infiltration rates in typical immersion tests (Liu, 2011; Ma et al., 2014; Wu, 2016).

subsidence curve was altered to pattern ④ from pattern ① as the water infiltrated to the depth of 20 m from 5 m. During this process, the decreasing difference value between the adjacent pattern lines indicated that the surface settlement gradually diminished with each 5 m increment of infiltration depth. However, the ground settlement and its influence scope increased dramatically during water permeation between the depths of 20 m and 25 m (from pattern ④ to ⑤), which arrived at the tunnel's burial depth. During this stage, the subsidence of the pit's central point was 19.4 cm, accounting for 35.9% of the final, total settlement. This result reflects the appearance of significant surface settlement development when the water infiltrated into the surrounding loess near by the tunnel vault. In addition, although the water continued to move downward, the surface settlement gradually stabilized. Finally, the maximum subsidence of the centre was 54 cm, and the horizontal scope impacted by the collapse was approximately 6 m away from the boundary of the trial pit, which forms a funnel shape (pattern ⑦).

3.2.3. Stratified settlement

Fig. 15 shows the variation curves of strata settlement at different depth ranges above the tunnel. From this diagram, the stratified subsidence successively moved from shallow to deep depths as the water infiltration depth increased, and the subsidence of each soil layer was obviously different. The settlement of the soil strata within the depth range of 10.7 m is large and accounts for more than 60% of the total settlement of entire stratum (Table 3). Although the stratum within the depth range of 5.5 m was wetted earlier, the settlement in this scope was less than that in the scope from 5.5 m to 10.7 m because of the limited overburden stress. The compactness of the natural soil increases with the increase in strata depth, and thus, the subsidence of the soil layer ranging from 10.7 m to 15.6 m obviously decreases to 12.2 cm, which accounts for only 8.4% of the total subsidence. However, the stratified settlement in the deeper strata, ranging from 15.6 m to 20.8 m and below 20.8 m, are greater than 12.2 cm respectively. The cumulative settlement of strata over the depth of 15.6 m is 45.4 cm, which accounts for 31.4% of the total settlement of the entire stratum.

The changing process of the strata settlement mentioned above reveals that an obvious subsidence formed in the surrounding loess within about a distance of one tunnel height above the tunnel vault. Due to the unloading effect caused by tunnel excavation, it was inferred that an unstable, loose body or a soil arching region formed above the tunnel vault. The surrounding loess reached a new equilibrium and maintained a relatively stable state after tunnel construction. During the process of water infiltration from the ground surface, especially when the water was close to the burial depth of the tunnel, the collapse deformation upon wetting and the compressive deformation caused by reloading occurred simultaneously in the unstable loose body, which is greater than the individually collapsible subsidence caused by wetting in the natural loess stratum without a tunnel. Therefore, the hydrocollapse of the deep loess was enhanced by the effects of disturbance during tunnel

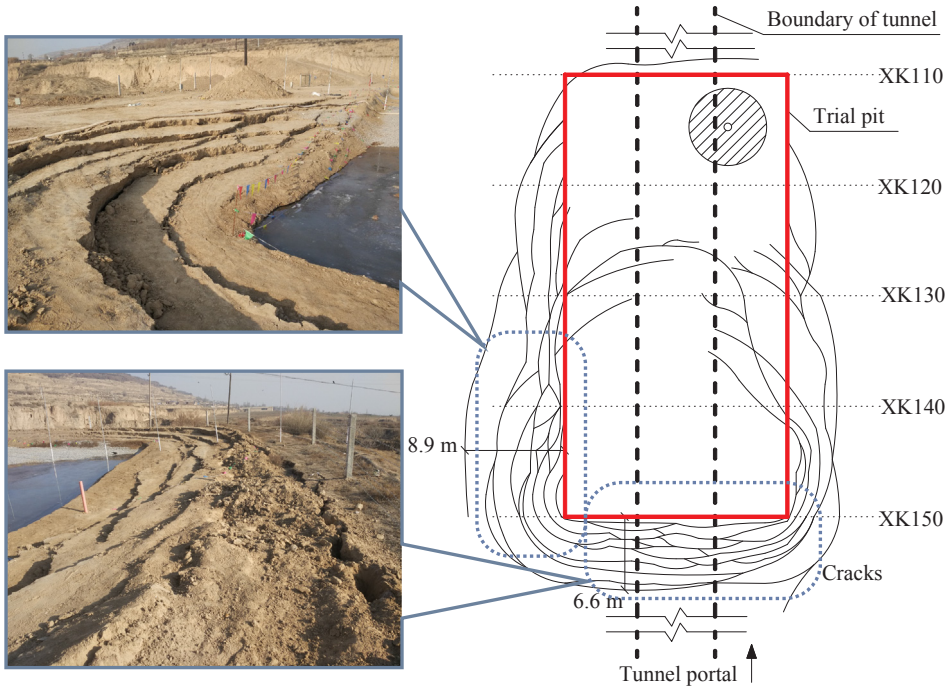

Fig. 13. Distribution pattern of cracks in ground surface (imaged by authors).

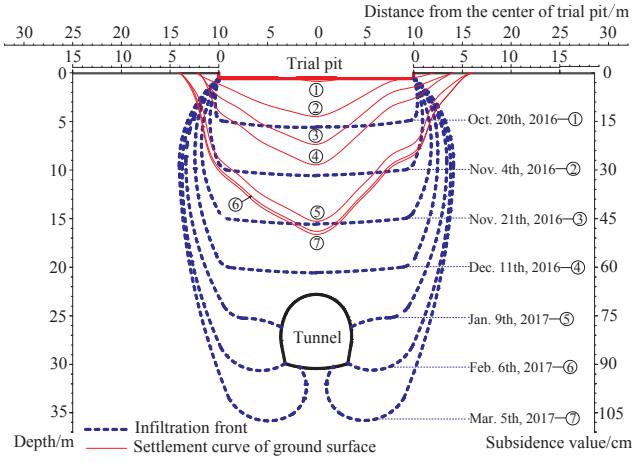

Fig. 14. Surface subsidence variation with water infiltration.

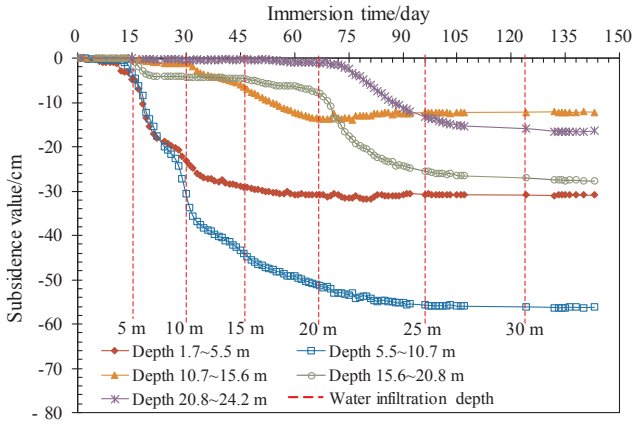

Fig. 15. Settlement process of soil layer distributed in different depths.

Table 3
Stratified settlement of soil layer above the tunnel.

Monitoring point label	Burial depth/m	Total settlement/cm	Range of depth/m	Stratified settlement/cm	Proportion/%
F1	1.7	144.7	1.7–5.5	30.9	21.4
F4	5.5	113.8	5.5–10.7	56.2	38.8
F5	10.7	57.6	10.7–15.6	12.2	8.4
F3	15.6	45.4	15.6–20.8	27.7	19.2
F7	20.8	17.7	Below 20.8	17.7	12.2

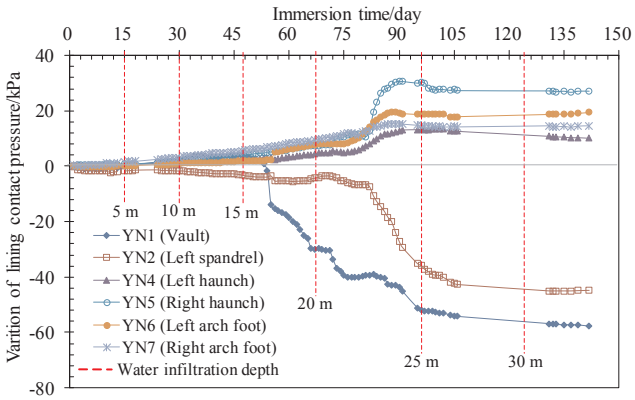

Fig. 16. Variation of contact pressure in the section of XK140.

excavation.

3.3. Mechanical response of tunnel structure

3.3.1. Contact pressure between the lining structures

Fig. 16 shows the variation in the contact pressure between the lining structures in section XK140 (burial depth of 20.9 m) during the immersion test. From Fig. 16, the development process of the contact pressure can be roughly divided into three stages: ① when the water

was infiltrating within the depth range of 15 m, the variation in contact pressure measured by each pressure cell was negligible. ② After the water infiltrated deeper than 15 m, the contact pressure at the tunnel vault decreased rapidly. ③ As the water infiltrated further, the contact pressure at the vault and spandrel continued to decrease, while the contact pressure at other monitoring locations showed incremental changes of differing degrees. During the entire course of the test, the maximum decrease of the contact pressure was 57.7 kPa and the maximum increase of the contact pressure was 30.6 kPa, which occurred at the vault and the right haunch of the tunnel, respectively.

This changing process indicates that during the initial stage of the immersion test, the surface water was permeating the stratum far from the tunnel vault, and there was almost no effect on the pressure state of the tunnel structure. As the water infiltrated close to the burial depth of the tunnel, the elastic resistance of the surrounding loess above the tunnel decreased upon wetting, which resulted in rebound deformation at the roof of the primary lining and a rapid decrease of contact pressure at the tunnel vault. After the water infiltration depth exceeded the burial depth, the stiffness of the surrounding loess on both sides of the tunnel was softened, which increased the lateral pressure sustained by the external sidewalls of the tunnel and the contact pressure at the haunches and arch feet. Meanwhile, under the squeezing action of the external sidewall, the dome of the tunnel structure continued to deform along the vertical direction, which resulted in a further decrease in the contact pressure at the vault and spandrel of the tunnel.

Although the change of the contact pressure was relatively small, it could reflect the deformation tendency of the primary lining under the collapsible effect of surrounding loess. The main change characteristic is that the sidewalls of the tunnel are squeezed laterally by the surrounding loess and the dome of the primary lining tends to move upward, which is shown in Fig. 17.

3.3.2. Base pressure and subsidence of the tunnel structure

Fig. 18 shows the variations in the base pressure under the inverted arch during the immersion test. Before the water infiltration arrived at the depth of 20 m, the base pressure increased slowly with an increment rate of less than 0.6 kPa/d. The base pressure increased dramatically once the water infiltrated close to the burial depth of the tunnel. The maximum increment of the base pressure in sections XK140 and XK120 were 277.5 kPa and 108.2 kPa, respectively.

As the water infiltrated close to the burial depth of the tunnel, the shear strength and bearing capacity of the surrounding rock above the tunnel decreased or even disappeared due to wetting, which significantly increased the surrounding rock pressure sustained by the tunnel structure. The incremental changes in the surrounding rock pressure and the weight of the water were transferred to the base by the

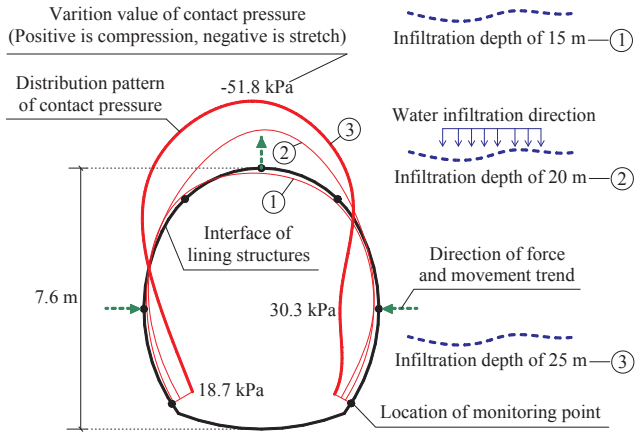

Fig. 17. Contact pressure on section XK140 changes with water infiltration depth.

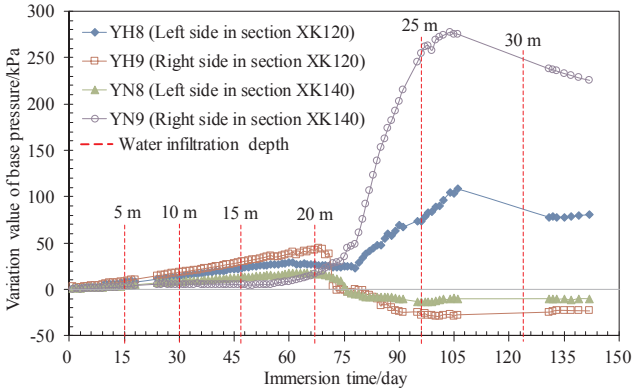

Fig. 18. Variations of base pressure in two sections.

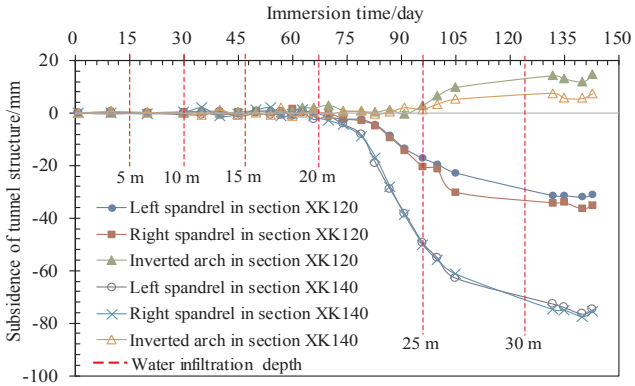

Fig. 19. Variations of tunnel subsidence in two sections.

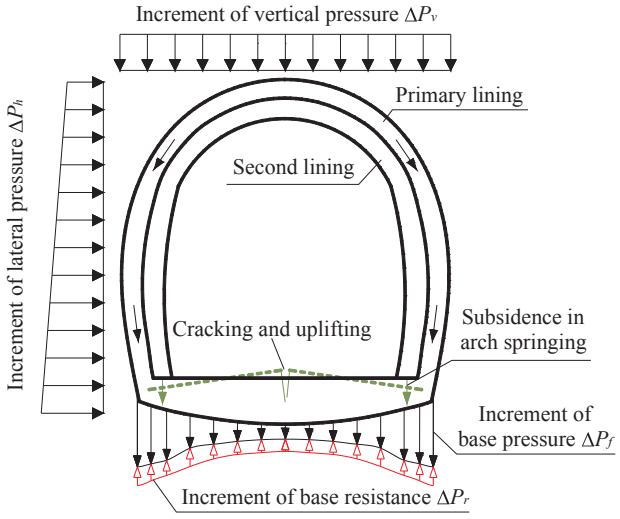

Fig. 20. Development process of tunnel subsidence and cracking.

tunnel structure, which significantly increased the base pressure. Because the burial depth of section XK140 was relative shallow and the collapsible deformation of the overlying strata above this section was more severe, the incremental changes in the base pressure in section XK140 were larger than those in section XK120.

The subsidence variation in the tunnel structure is shown in Fig. 19. The tunnel subsidence changes correspond with the base pressure variation mentioned above. In the early stage of the immersion test, the incremental changes in the base pressure were small, and no subsidence occurred in the tunnel structure. When the water infiltration arrived at the burial depth of the tunnel, the second lining began to sink, the

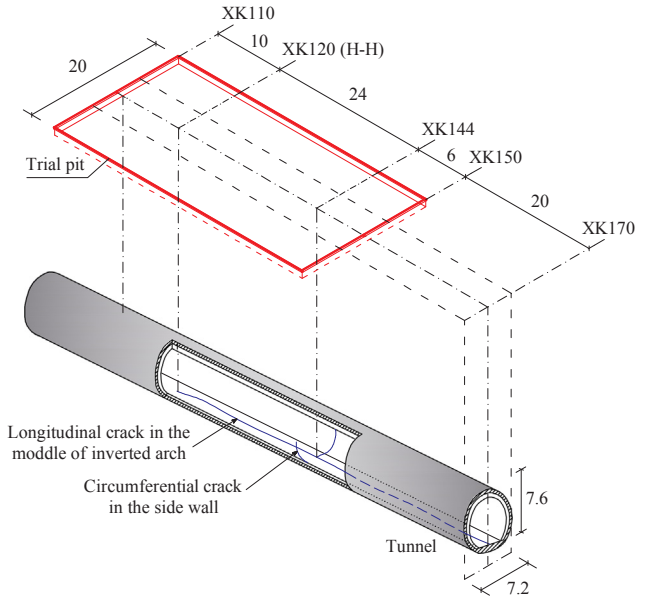

Fig. 21. Diagram of the distribution of cracks in the tunnel (unit: m).

subsidence increased with the increase in base pressure, and a slight uplift occurred at the central part of the inverted arch. Finally, the overall subsidence of the second lining in sections XK140 and XK120 were 75 mm and 35 mm, and the uplift deformations of the inverted arches in the two sections were 7.4 mm and 14.5 mm, respectively.

The base pressure distribution under the tunnel was uneven, the stress concentration formed under the arch feet due to the shape shifting of the tunnel section. Plastic zones easily formed in the foundation soil under the arch feet during the tunnel construction, which decreased the bearing capacity of the foundation in this zone. Thus, under the continuous increase in base pressure and the softening of the soil stiffness upon wetting, significant subsidence occurred at the arch feet, which caused the overall subsidence of the second lining structure. However, because of the unloading effect of the tunnel excavation, the base pressure in the central part of the inverted arch was relatively small and was generally less than the original gravity stress. The subsidence of the tunnel in this zone was inhibited by the elastic resistance of the foundation soil. As a result, a longitudinal crack was generated in the middle of the inverted arch under the effect of differential settlement between the arch foot and the central part of the inverted arch. With further development of differential settlement, slight uplift occurred at the central part of the inverted arch because of the integral rigidity of the structure on both sides of the crack, and the crack gradually expanded until the subsidence was stable. Fig. 20 shows the formation process of the subsidence and the longitudinal crack in the inverted arch of tunnel.

Eventually, the maximum width of the longitudinal crack reached 4 cm, and the total length was approximately 50 m, which was distributed between the tunnel mileages from XK120 to XK170. Furthermore, because of the differential settlement of the surrounding rock along the longitudinal direction of the tunnel, a circumferential crack appeared in the sidewall of the second lining in section XK144, which ranged from the haunch of the tunnel to the inverted arch, as shown in Figs. 21 and 22.

Therefore, for a loess tunnel with a relatively shallow burial depth, to prevent the threat of surface water on the safety of the tunnel structure, long-term immersion on the ground surface above the tunnel should be avoided. Especially for obvious settlement or crevices appearing on the ground surface during tunnel construction, the path of water infiltration is more unobstructed. The cracks on the ground surface should be treated in time and it is necessary to supply waterproofing and drainage measures in the corresponding areas. In addition, the possibility of a bearing capacity decrease and subsidence of the tunnel foundation at the arch feet caused by wetting should be fully considered in the design and construction of loess tunnel engineering. The central cracking caused by differential settlement may be eliminated by enhancing the transverse tensile stiffness of the inverted arch structure.

4. Conclusions

In this study, by performing a field water immersion test on the ground surface above a loess tunnel, the water infiltration pattern and collapsible deformation behaviour of the loess tunnel site and the mechanical response of the tunnel structure were investigated. The major conclusions are summarized below.

(1) Compared with natural loess sites, the existence of a loess tunnel

Fig. 22. Cracks on the tunnel structure (imaged by authors).

significantly increases the depth of water seepage from the ground surface. For a loess tunnel with a relatively shallow burial depth, during the process of long-term immersion on the ground surface above the tunnel, the water mainly permeates along the vertical direction and gradually infiltrates to the tunnel burial depth or even to the base of the tunnel. In this study, the maximum water infiltration depth was 35 m, which exceeded the depth of the tunnel base, and the final infiltration scope caused by the surface water formed the shape of a 'lamp bulb'.

(2) The natural structure of the surrounding loess was disturbed by the tunnel excavation, which increased the hydrocollapse of the deep loess. Once the surface water infiltrated close to the burial depth of the tunnel, the collapse deformation caused by wetting and the consolidation caused by reloading occurred simultaneously in the surrounding loess, which was greater than the collapsible subsidence in the natural loess stratum.

(3) The surface water that permeates within the shallow stratum has less impact on the tunnel structure. The pressure state of the tunnel structure will be changed due to the hydrocollapse of the surrounding loess once the surface water infiltrates close to the burial depth of the tunnel. The main characteristic of change is that the sidewalls of the tunnel are squeezed laterally by the surrounding loess and the vault of the primary lining has the tendency to move upward.

(4) As surface water infiltrates to the tunnel burial depth, the base pressure, especially under the arch feet, will increase remarkably. The insufficient bearing capacity of the foundation causes obvious sinking at the arch feet, resulting in overall subsidence in the lining structure. However, the base pressure in the central part of the inverted arch is relatively small, and the subsidence of the tunnel in this zone is inhibited by the elastic resistance of the foundation soils. As a consequence, a longitudinal crack is generated in the middle of the inverted arch due to the differential settlement between the arch foot and the central part of the inverted arch.

Acknowledgements

This research project was financially supported by the National Natural Science Foundation of China (Grant numbers 41272320, 11572245, 51608442).

Appendix A. Supplementary data

Supplementary data associated with this article can be found, in the online version, at https://doi.org/10.1016/j.tust.2018.08.035.

References

Assallay, A.M., Rogers, C.D.F., Smalley, I.J., 1997. Formation and collapse of metastable particle packings and open structures in loess deposits. Eng. Geol. 48 (1–2), 101–115.

Cristi, F., Fierro, V., Suárez, F., 2016. A TDR-waveform approach to estimate soil water content in electrically conductive soils. Comput. Electron. Agric. 121, 160–168.

Derbyshire, E., Dijkstra, T.A., Smalley, I.J., 1994. Failure mechanisms in loess and the effects of moisture content changes on remoulded strength. Quat. Int. 24, 5–15.

Derbyshire, E., Meng, X.M., Wang, J.T., Zhou, Z.Q., Li, B.X., 1995. Collapse loess on the Loess Plateau of China. In: Derbyshire, E., Dijkstra, T., Smalley, I.J. (Eds.), Genesis and properties of Collapsible Soils. Kluwer, Dordrecht, pp. 267–293.

Derbyshire, E., 2001. Geological hazards in loess terrain, with particular reference to the loess areas of China. Earth-Science Review 54 (1–3), 231–260.

Haeri, S.M., Khosravi, A., Garakani, A.A., et al., 2016. Effect of soil structure and disturbance on hydromechanical behavior of collapsible loessial soils. Int. J. Geomech. 17 (1), 04016021.

Houston, S.L., Houston, W.N., Spadola, D.J., 1988. Prediction of field collapse of soils due to wetting. Journal of Geotechnical Engineering 114 (1), 40–58.

Huang, X.F., Liu, C.L., Yao, Z.H., et al., 2012. Study of infiltration and collapsible deformation law of unsaturated loess under over burden pressure by using TDR soil water probe. Rock Mech. Eng. 31 (supp 1), 3231–3238 (in Chinese).

Huang, X.F., Yang, X.H., 2013. A study progress on in-situ soaking test on collapsible loess. Rock Soil Mech. 34 (Supp. 2), 222–228 (in Chinese).

Huang, X.H., 2017. Study on the tunnel lining mechanical behavior induced by longitudinal local collapsibisity of loess tunnel foundation.MS Thesis. Southwest Jiaotong University (in Chinese), Chengdu, China.

Li, P., Vanapalli, V., Li, T.L., 2016. Review of collapse triggering mechanism of collapsible soils due to wetting. J. Rock Mech. Geotech. Eng. 8 (2), 256–274 (in Chinese).

Li, G.L., Shao, S.J., Jin, B.C., et al., 2015. Research on the problems of collapsibility of loess tunnel foundation. J. Railway Eng. Soc. 12, 12–16 (in Chinese).

Lin, X.W., Wang, J., Wang, L.X., Zhang, Y.W., 2016. Experimental research on influence of loess collapsibility on subway tunnels. Chinese J. Geotech. Eng. 38 (8), 1374–1380 (in Chinese).

Liu, T.S., Chang, T.H., 1964. The 'huangtu' loess of China. Report of the Sixth INQUA Congress, Warsaw 1961, vol. 4, pp. 503–524.

Liu, C.L., 2011. A study on the law of permeability and collapsibility deformation and evaluation of collapsible of big thickness loess collapsible under over burden pressure. MS. Thesis. Lanzhou University of Technology (in Chinese), Lanzhou, China.

Ma, Y., Wang, J.D., Peng, S.J., et al., 2014. Immersion tests on characteristics of deformation of self-weight collapsible loess under overburden pressure. Chinese J. Geotech. Eng. 36 (3), 537–546 (in Chinese).

MCPRC (Ministry of Construction of the People's Republic of China), 2004. Code on building construction in regions of collapsible loess (GB 50025–2004). China Building Industry Press, Beijing (in Chinese).

Shao, S.J., Li, J., Li, G.L., et al., 2015. Evaluation method for self-weight collapsible deformation of large thickness loess foundation. Chinese J. Geotech. Eng. 37 (6), 965–978 (in Chinese).

Shao, S.J., Yang, C.M., Jiao, Y.Y., Lu, S., 2013. Engineering properties of collapsible loess tunnel. Chinese J. Geotech. Eng. 35 (9), 1580–1590 (in Chinese).

Shao, S.J., Chen, F., Shao, S., 2017. Collapse deformation evaluation method of loess tunnel foundation. Chinese J. Rock Mech. Eng. 36 (5), 1289–1300 (in Chinese).

Sun, P.P., Zhang, M.S., Zhu, L.F., 2013. Typical case study of loess collapse and discussion on related problems. Geol. Bull. China 32 (6), 847–851 (in Chinese).

Tian, S.M., 2017. Study on mechanical properties of surrounding rock in circle partial collapse around loess tunnel.MS Thesis. Southwest Jiaotong University (in Chinese), Chengdu, China.

Wang, X.L., Zhu, Y.P., Huang, X.F., 2014. Field tests on deformation property of self-weight collapsible loess with large thickness. Int. J. Geomech. 14 (3), 04014001.

Wu, X.P., 2016. Study on the characteristics of collapse and permeability of large thickness loess ground based on water immersion test. PD. Thesis. Lanzhou University (in Chinese), Lanzhou, China.

Xie, D.Y., 2001. Exploration of some new tendencies in research of loess soil mechanics. Chinese J. Geotech. Eng. 23 (1), 3–13 (in Chinese).

Yao, Z.H., Huang, X.F., Chen, Z.H., et al., 2012. Comprehensive soaking tests on self-weight collapse loess with heavy section in Lanzhou region. Chinese J. Geotech. Eng. 34 (1), 65–74 (in Chinese).

Yao, Z.H., Huang, X.F., Chen, Z.H., et al., 2014. New recognition of collapsibility evaluation and remnant collapse of loess. Rock Soil Mech. 35 (4), 998–1005 (in Chinese).